Analytical treatment for cyclic three-state dynamics on static networks

Chao-Ran Cai [1,2,*] and Zhi-Xi Wu [3,†]
[1]*School of Physics, Northwest University, Xi'an 710069, China*
[2]*Shaanxi Key Laboratory for Theoretical Physics Frontiers, Xi'an 710069, China*
[3]*Institute of Computational Physics and Complex Systems, Lanzhou University, Lanzhou, Gansu 730000, China*

(Received 28 May 2019; published 21 January 2020)

Whenever a dynamical process unfolds on static networks, the dynamical state of any focal individual will be exclusively influenced by directly connected neighbors, rather than by those unconnected ones, hence the arising of the dynamical correlation problem, where mean-field-based methods fail to capture the scenario. The dynamic correlation coupling problem has always been an important and difficult problem in the theoretical field of physics. The explicit analytical expressions and the decoupling methods often play a key role in the development of corresponding field. In this paper, we study the cyclic three-state dynamics on static networks, which include a wide class of dynamical processes, for example, the cyclic Lotka-Volterra model, the directed migration model, the susceptible-infected-recovered-susceptible epidemic model, and the predator-prey with empty sites model. We derive the explicit analytical solutions of the propagating size and the threshold curve surface for the four different dynamics. We compare the results on static networks with those on annealed networks and made an interesting discovery: for the symmetrical dynamical model (the cyclic Lotka-Volterra model and the directed migration model, where the three states are of rotational symmetry), the macroscopic behaviors of the dynamical processes on static networks are the same as those on annealed networks; while the outcomes of the dynamical processes on static networks are different with, and more complicated than, those on annealed networks for asymmetric dynamical model (the susceptible-infected-recovered-susceptible epidemic model and the predator-prey with empty sites model). We also compare the results forecasted by our theoretical method with those by Monte Carlo simulations and find good agreement between the results obtained by the two methods.

DOI: 10.1103/PhysRevE.101.012305

I. INTRODUCTION

Networked cyclic three-state dynamics are frequently used as important models in the field of ecology [1–3] and sociology [4,5]. Each node in the network is considered to be in one of the three possible states (e.g., rock, paper, and scissor) at each moment of time. The selected node change its state stochastically, from one state (scissor) to another state (rock), with a probability dependent on the states of the node itself and its neighbors. Concrete examples include theoretical models for competing species in ecosystems, the so-called cyclic Lotka-Volterra model [6–9] or predator-prey model [10–12]. Models for rumor propagation, popularization of new technologies and products, and transmission of neural signals can be casted into the classical susceptible-infected-recovered-susceptible (SIRS) epidemic model [13,14].

Generally, we can interpret the three states in the context of various scenarios, ranging from strategies in the rock-paper-scissors games [15,16], over tree, burning tree, empty site in the forest-fire model [17,18], to bacterial species adopting different survival strategies [19–24]. In particular, Sinervo and Livdy studied territory use and patterns of sexual selection in male side-blotched lizard populations [22] and found that the large territories strategy of orange males is defeated by the "sneaker" strategy of yellow males, which is in turn defeated by the mate-guarding strategy of blue males; the large territories strategy defeats the mate-guarding strategy to complete the dynamic cycle. The authors of Refs. [19,20] have investigated the coexistence mechanism among three populations of *Escherichia coli* by experiments *in vitro* and *in vivo*, respectively. In these studies, sensitive strains beat resistant strains due to a growth-rate advantage, resistant strains beat colicinogenic strains also by a growth-rate advantage, and colicinogenic strains displace sensitive strains by killing them, these three populations of *E. coli* also satisfies a cyclic dynamical relationship.

In the literature of ecology, interest is often focused on the mechanisms of species coexistence or extinction [25–27], and that is often focused on the disease breakout or not in networked epidemiology [28–31], whose dynamics resembles like the phenomenon of phase transition in the field of statistical physics [32–35]. Most theoretical researches based on the Lotka-Volterra model, which are used to interpret the corresponding experiments, were exclusively focused on the dynamical behavior itself, and did not take into account the spatial structure or the details of interaction among species [6,7,24,27,36,37]. Under such scenario, the dynamics of the model can be regarded as taking place on annealed networks, where each node has the equal probability to interact with everyone others.

However, the living space of species has generally a geographical spatial structure [9,38], which is inappropriately

*ccr@nwu.edu.cn
†wuzhx@lzu.edu.cn

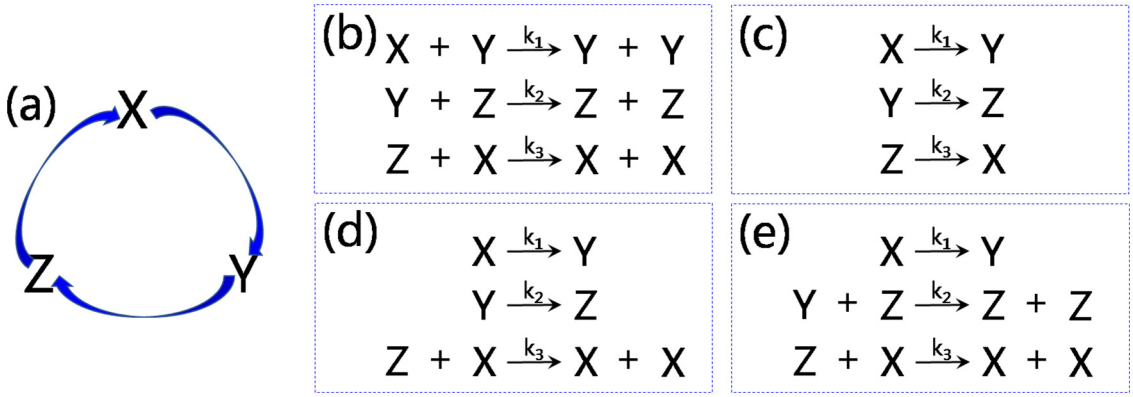

FIG. 1. (a) Schematic illustration of the transition events of the cyclic three-states dynamics model. (b) The cyclic Lotka-Volterra model. (c) The directed migration model. (d) The susceptible-infected-recovered-susceptible epidemic model. (e) The predator-prey model with empty sites model. For a brief and convenient formulation, in the cyclic three-state dynamics, we use k_1, k_2, k_3 to replace the $k_{l\to m}$ in the derivations of explicit analytical solutions.

represented by annealed networks in the global scale, though due to the natural factor (wind and rain) and animal behavior (mobility), long-range interactions among species may frequently appear. To fully understand the picture of the cyclic interactions among species, it is undoubtedly necessary to study how cyclic three-state model behaves on static topology.

For a static spatial network, a node transfers its state (which can be interpreted as information, strategy, disease, territory dominator, and so on) to other nodes just by a set of fixed paths. For example, a susceptible individual can only be infected by its infectious neighbors. Meanwhile, predators generally use a fixed and the most efficient feeding behavior, and do not change the home range frequently [39]. That is to say, the state of each node is related to those of its neighbors. In this paper, we investigate from coupled ordinary differential equations over dynamic correlations to explicit analytical solutions in cyclic three-states dynamics on spatial static networks. And we will show below that our analytical solutions, including the value of steady state and phase transition point, are in good agreement with those by the Monte Carlo simulations.

The remainder of paper is organized as follows. In Sec. II, we show the four typical kinds of three-state dynamical models, the generation of static networks, and other parametrizations to help readers understanding this work easily. In Sec. III, we present the derivations of the coupled ordinary differential equations with multiple-state dynamics on static networks. In Sec. IV, we give the derivations of analytical solutions for the four different cyclic three-state dynamics on static networks. Finally, in Sec. V, we discuss the results and conclude the paper. Details of some mathematical derivations are contained in the Appendices.

II. MODEL

A. Typical representations of three-state model

The cyclic three-state dynamics model constitutes the following interactions: three states X, Y, and Z cyclically dominate each other, that is, X beats Y beats Z beats X, see Fig. 1(a) for a graphical illustration. For simplicity and without loss of generality, we consider two of the simplest types of interactions in a population, whose outcome is either only dependent on the state of the node itself, which will be named as "intrinsic interaction" (e.g., the infected individual heal to a recovered state), or rely on the states of its neighbors explicitly, which is termed as "neighbor interaction" (e.g., the susceptible individual can be infected by its infectious neighbors).

We denote $A_{l\to m}$ as the total rate of a node which changes its state l to state m, where $l, m \in \{X, Y, Z\}$. And we have

$$A_{l\to m} = \begin{cases} k_{l\to m} a_m, & \text{neighbor interaction,} \\ k_{l\to m}, & \text{intrinsic interaction,} \end{cases} \tag{1}$$

where $k_{l\to m}$ is the rate of interaction from state l to state m, and a_m is the number of state m from the neighbors of the selected node. Now, four possible dynamical processes are included in our general model. Specifically, Fig. 1(b) corresponds to the cyclic Lotka-Volterra model, where all reaction processes are based on neighbor interactions [6–8]. Figure 1(c) depicts a directed migration model, which characterizes the migration process of animals among three adjacent habitats (here $\{X, Y, Z\}$ denote the magnitude of the biomass on the habitats). If only one neighbor interaction occurs and the other two are intrinsic interactions [Fig. 1(d)], then we yield the SIRS model [13] (where Z, X, and Y corresponds to the states S, I and R, respectively), or forest-fire model [40] (where Z, X, and Y corresponds to the states of "tree," "burning tree," and "vacant site," respectively). In Fig. 1(e), there exist two intrinsic interactions and one neighbor interaction among $\{X, Y, Z\}$, which can be regarded as a predator-prey model with empty sites [10,41].

B. Static networks generation, stochastic simulation procedure, and other parameterizations

In this work, we solve analytically the four typical dynamical processes on static complex networks with three different degree distributions: Bimodal distribution $P(k) \sim g\delta(k-d_1) + h\delta(k-d_2)$, where d_1 and d_2 are the two possible degree for any node in the network and $\frac{g}{g+h}$ (or $\frac{h}{g+h}$) is the proportion of nodes with degree d_1 (or d_2), respectively; Poisson distribution $P(k) \approx \exp^{-\langle k\rangle}\langle k\rangle^k/k!$, where $\langle k\rangle$ is the

average degree of an Erdős-Rényi (ER) random network; power-law distribution $P(k) \sim k^{-\gamma}$, where γ is the power exponent of a scale-free(SF) random network. For simplicity, we currently do not consider the effect of degree-correlation on the dynamical processes, and therefore use the uncorrelated configuration model algorithm presented in Ref. [42] to generate static networks.

We use the stochastic algorithm in Ref. [43] to simulate the four dynamical processes on static networks. The simulation procedure works as follows:

Step 1: Initialize the whole population and set time to zero.

Step 2: Calculate each state's interaction rate p_l. The interaction rate of a node with neighbor interaction is $p_l = k_l \times k_{\max}$. The interaction rate of a node with intrinsic interaction is $p_l = k_l$.

Step 3: Sample the length of this time step from an exponential distribution with parameter $\lambda = \sum_l (p_l \times L)$, where L is the number of subpopulation with state l and λ the total transition rate.

Step 4: Choose a subpopulation to performing possible state-transformation with a probability proportional to $(p_l \times L)$. Here, all nodes in the selected subpopulation with a specified state have the same probability to be selected and change their states.

Step 5: Randomly select a node i from the selected subpopulation. If the transition event is an intrinsic interaction, then the event happens deterministically ($X \to Y$ or $Y \to Z$ or $Z \to X$, for instance). If the transition event is a neighbor interaction, then it might happen with a probability of $k_i/k_{\max}$, where k_i is the degree of the selected node. In such case, node i still needs to take into account the following two steps: (i) One nearest neighbor j of the node i is randomly chosen; (ii) if node j is from state Y (Here, we assume that the state of node i is of state X), then node i changes its state from X to Y, else nothing happens.

Step 6: Update the sets of the three types of subpopulation, and repeat Steps 3–5 until the predetermined time period is reached.

Unless otherwise explicitly stated, we fix from now on the total population size as $N = 10^5$ (the number of nodes in the underlying interaction network), the average degree $\langle k \rangle$ of the ER networks as 4, and the minimum degree $k_{\min}$ and the power exponent γ of SF networks as 3 and 2.8, respectively. We choose $d_1 = h = 4$ and $d_2 = g = 10$ for the bimodal networks to guarantee that the connection probability is the same in the two different degrees. The initial proportion of subpopulation with different states $\{X, Y, Z\}$ are $X = 0.8$, $Y = 0.1$, and $Z = 0.1$, respectively. In this study, our key quantities are the proportion of different types of subpopulations in the steady state and the threshold curved surface of the coexistence of all states or not.

III. EFFECTIVE DEGREE APPROACH

The effective degree (ED) approach [44–48] (also known as the approximate master equations [49,50]), taking into consideration explicitly the dynamic correlations between directly connected neighbors, is a higher-order degree-based mean-field approach, which has widely been used in the studies of binary-states dynamics on networks. We here extend the ED approach to address multiple-states dynamics. Let us consider the problem of diversity of species in an ecosystem [25,26,38,51], wherein n species (states) can be denoted by $X_i (i = 1, 2, \cdots, n)$. The number of nodes of the state X_l, whose neighbors' states are $\{a_1, \cdots, a_n\}$, can be represented as $[X_l]_{\{a_1,\cdots,a_n\}}$, where a_i is the number of state X_i in the neighborhood of the node with state X_l. Consider an event that one node with the state X_l changes to the state X_m, the transition rate of the selected node can be calculated by using Eq. (1). The key point of the ED approach is to calculating, beyond the selected node's state itself, also the variation of the state transformation of those neighbors of the selected node, thanks to its state transformation. To be more specific, the analytical procedure is summarized as follows:

(1) We first calculate the total rate of the new arrival state X_m, whose value is $\sum_{\{a_1,\cdots,a_n\}} A_{l\to m}[X_l]_{\{a_1,\cdots,a_n\}}$, where $\sum_{\{a_1,\cdots,a_n\}}$ means that we sum over all possible a_i.

(2) Consider the neighbors' state information of the selected node, we know that the total rate of state X_s nodes whose effective degrees are changed by these new arrival state X_m is $\sum_{\{a_1,\cdots,a_n\}} A_{l\to m}[X_l]_{\{a_1,\cdots,a_n\}} a_s$.

(3) The total number of X_l neighbors of state X_s nodes is $\sum_{\{a_1,\cdots,a_n\}} [X_s]_{\{a_1,\cdots,a_n\}} a_l$.

(4) We define $B_{l\to m,s}$ as the rate of one state X_s node to change its effective degree because of a transition event that one state X_l node transform to state X_m, and $B_{l\to m,s} = \frac{\sum_{\{a_1,\cdots,a_n\}} A_{l\to m}[X_l]_{\{a_1,\cdots,a_n\}} a_s}{\sum_{\{a_1,\cdots,a_n\}} [X_s]_{\{a_1,\cdots,a_n\}} a_l}$.

With these quantities at hand, the dynamic coupled ordinary differential equations in the framework of the ED approach are given by

$$\begin{aligned}\frac{d[X_j]_{\{a_1,\cdots,a_n\}}}{dt} = &-\sum_{i=1}^{n}\left\{[X_j]_{\{a_1,\cdots,a_n\}} A_{j\to i}\right\} \\ &+\sum_{i=1}^{n}\left\{[X_i]_{\{a_1,\cdots,a_n\}} A_{i\to j}\right\} \\ &+\sum_{l=1}^{n}\sum_{m=1,\neq l}^{n}\left\{[(a_l+1)[X_j]_{\{\cdots,(a_l+1),\cdots,(a_m-1)\cdots\}} \right. \\ &\left. - a_l [X_j]_{\{a_1,\cdots,a_n\}}] B_{l\to m,j}\right\}. \end{aligned} \tag{2}$$

It is easy to see that the total number of differential equations are proportional to $k_{\max}^n$.

IV. ANALYTICAL TREATMENT AND NUMERICAL SIMULATION OF THE THREE-STATE DYNAMICAL PROCESSES

In what follows, we present the analytical treatment of the three-state dynamical processes on static networks. For convenience, we use k_1, k_2, k_3 to replace the $k_{X\to Y}$, $k_{Y\to Z}$, and $k_{Z\to X}$ in the derivations of differential equations.

To begin, by following a randomly chosen edge from X-state nodes of degree k, we define the probabilities of reaching an arbitrary node with state X, state Y, and state Z are P_{kx1}, $(1 - P_{kx1})P_{kx2}$, $(1 - P_{kx1})(1 - P_{kx2})$, respectively. Then, X_{abc} can be written as

$$X_{abc} = X_k \binom{k}{a} P_{kx1}^a (1 - P_{kx1})^{k-a} \binom{b+c}{b} P_{kx2}^b (1 - P_{kx2})^c,$$

where X_{abc} is the number of nodes of the state X, whom in the mean time have a neighbors with state X, b neighbors with state Y, and c neighbors with state Z, $k = a + b + c$ is the total degree of the focal node, and $X_k = \sum_{k=a+b+c} X_{abc}$ is the number of nodes with state X and degree k. Similarly, by following a randomly chosen edge from nodes of degree k and with Y state (or Z state), we define the probabilities of reaching an arbitrary node with state X and state Z node are P_{ky1} (or P_{kz1}) and $(1 - P_{ky1})P_{ky2}$ [or $(1 - P_{kz1})P_{kz2}$], respectively. With these definitions we are able to decouple the dynamic correlation from directly connected neighbors by the relationships of $\sum_i \binom{j}{i} P^i (1-P)^{j-i} i = jP$ and $\sum_i \binom{j}{i} P^i (1 - P)^{j-i} i^2 = j(j-1)P^2 + jP$.

By far, the dimensionality of the coupling differential equations is very high. Here, we use the ED approximate condition to reduce it by concerning about the properties of the system in the steady state. In particular, the analytical procedure can be performed as follows:

(1) In a static network, we calculate the probability of connecting an arbitrary X-state node by an X-state node i, P_{kx1}, which is equivalent to calculate the probability of each neighbor of the node i to becoming state X.

(2) The effective degree approach just consider explicitly the dynamic correlations between directly connected neighbors (see Sec. III). Here, for one nearest neighbor j of the node i, the probability of changed its state just is concerned with neighbors' state of node j itself under the ED approximate condition.

(3) That is to say, the value P_{kx1} is thought to be independent of the degree of node i in the framework of the ED approach.

So, we can simplify the values of $P_{x1}, P_{x2}, P_{y1}, P_{y2}, P_{z1}, P_{z1}$, which can be approximated as [47]

$$P_{1D} \simeq P_{2D} \simeq \cdots \simeq P_{kD} \simeq \cdots \simeq P_{k_{\max} D} = P_D, \tag{3}$$

where $D \in \{x1, x2, y1, y2, z1, z2\}$.

Since the interaction structure among the nodes is fixed in the static networks, the total number of M-state neighbors of all L-state nodes equals to the total number of L-state neighbors of all M-state nodes, that is

$$\begin{aligned}
\sum_k \sum_{k=a+b+c} bX_{abc} &= \sum_k \sum_{k=a+b+c} aY_{abc}, \\
\sum_k \sum_{k=a+b+c} cX_{abc} &= \sum_k \sum_{k=a+b+c} aZ_{abc}, \\
\sum_k \sum_{k=a+b+c} cY_{abc} &= \sum_k \sum_{k=a+b+c} bZ_{abc},
\end{aligned}$$

which always holds and is independent on the type of dynamical processes. Plugging Eq. (3) into the above equation, we yield

$$\begin{aligned}
\frac{\sum_k kX_k}{\sum_k kY_k} &= \frac{P_{y1}}{P_{x2}(1 - P_{x1})}, \\
\frac{\sum_k kX_k}{\sum_k kZ_k} &= \frac{P_{z1}}{(1 - P_{x1})(1 - P_{x2})}, \\
\frac{\sum_k kY_k}{\sum_k kZ_k} &= \frac{P_{z2}(1 - P_{z1})}{(1 - P_{y1})(1 - P_{y2})}.
\end{aligned} \tag{4}$$

TABLE I. All possible event in an interval time dt of the cyclic three-state dynamic model on a static network. For the cyclic Lotka-Volterra model, $(A_{X\to Y}, A_{Y\to Z}, A_{Z\to X}) = (bk_1, ck_2, ak_3)$; for the directed migration model, $(A_{X\to Y}, A_{Y\to Z}, A_{Z\to X}) = (k_1, k_2, k_3)$; for the susceptible-infected-recovered-susceptible epidemic model, $(A_{X\to Y}, A_{Y\to Z}, A_{Z\to X}) = (k_1, k_2, ak_3)$; for the predator-prey with empty sites model, $(A_{X\to Y}, A_{Y\to Z}, A_{Z\to X}) = (k_1, ck_2, ak_3)$. $\lambda = \sum_{abc}(X_{abc}A_{X\to Y} + Y_{abc}A_{Y\to Z} + Z_{abc}A_{Z\to X})$.

Event	Probability	ΔX	ΔY	$\Delta[XY]$	$\Delta[XZ]$	$\Delta[YZ]$
$X_{abc} \to Y_{abc}$	$X_{abc}A_{X\to Y}/\lambda$	-1	$+1$	$a - b$	$-c$	c
$Y_{abc} \to Z_{abc}$	$Y_{abc}A_{Y\to Z}/\lambda$	0	-1	$-a$	a	$b - c$
$Z_{abc} \to X_{abc}$	$Z_{abc}A_{Z\to X}/\lambda$	$+1$	0	b	$c - a$	$-b$

At any time, one happened event will cause a small perturbation among the number of nodes with different states as well as the edges connecting different states in the network. When the system evolves to its steady state, the statistical quantities, such as the number of nodes with X state and the number of edge $[XY]$ (connecting a pair of nodes with state X and Y), are in dynamic equilibrium. We denote ΔL and $\Delta[LM]$, where $L, M \in \{X, Y, Z\}$, as the variation of the number nodes with L-state and that of the $[LM]$ edge in the time interval dt (where only one event occurs) in the population. All possible values of these quantities on a static network are summarized in Table I.

Combining the detailed balance condition of nodes' state and edge's state in the stationary state with Eqs. (3) and (4), we can obtain the explicit analytical solution in cyclic three-states dynamics on spatial static networks.

A. The cyclic Lotka-Volterra model

We first consider the cyclic Lotka-Volterra model [6–8], which include all the three neighbor interaction processes as shown in Fig. 1(b). In Fig. 2, it is obvious that there is an excellent agreement between the numerical solutions of Eqs. (1) and (2) and the stochastic simulation results, for the time series of the proportion of different types of subpopulations, both during the relaxation process and in the steady state.

Next, we derive the analytical solutions in static networks by solving the dynamic correlation problem in the steady state. Consider the detailed balance condition of nodes' state in the stationary state, $\langle \Delta X \rangle = \langle \Delta Y \rangle = 0$, we have

$$\sum_{abc} X_{abc} bk_1 = \sum_{abc} Z_{abc} ak_3 = \sum_{abc} Y_{abc} ck_2,$$

where $\sum_{abc}$ means summing over all subscripts. Plugging Eq. (3) into the above equation, we yield

$$\begin{aligned}
\frac{\sum_k k_1 kX_k}{\sum_k k_3 kZ_k} &= \frac{P_{z1}}{P_{x2}(1 - P_{x1})}, \\
\frac{\sum_k k_1 kX_k}{\sum_k k_2 kY_k} &= \frac{(1 - P_{y1})(1 - P_{y2})}{P_{x2}(1 - P_{x1})}, \\
\frac{\sum_k k_3 kZ_k}{\sum_k k_2 kY_k} &= \frac{(1 - P_{y1})(1 - P_{y2})}{P_{z1}}.
\end{aligned} \tag{5}$$

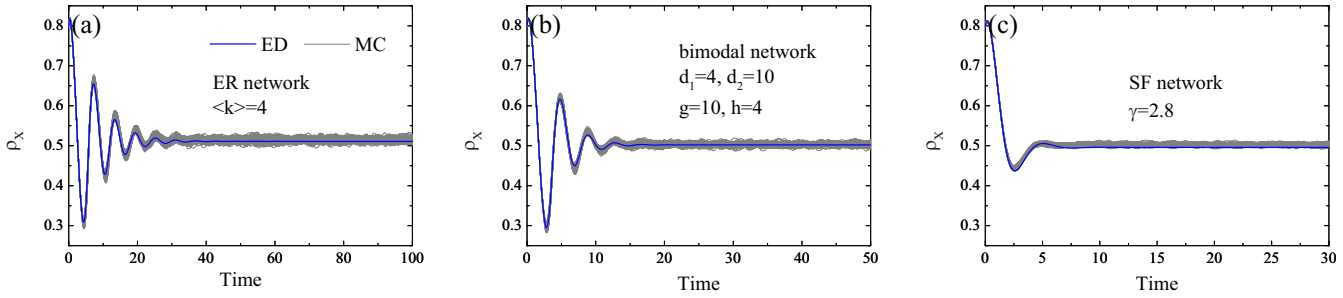

FIG. 2. Comparison of the results obtained by Monte Carlo simulations and by the effective degree approach for the cyclic Lotka-Volterra model on static networks with different degree distributions. The fraction of X-state nodes, ρ_x, as a function of the time are explicitly shown for comparison. Thick blue solid lines are the numerical solutions of Eqs. (1) and (2) and thin gray lines are 100 independent runs of simulation results. Parameters: $k_1 = 0.3$, $k_2 = 1.0$, $k_3 = 0.7$.

After eliminating X_k, Y_k, and Z_k from Eqs. (5) and (4), we readily obtain the value of P_{x2}, the relationship of P_{y1} and P_{y2}, and the relationship of P_{z1} and P_{z2} as

$$\begin{aligned} P_{x2} &= k_3/(k_1+k_3), \\ (1-P_{y1})(1-P_{y2})k_2 &= P_{y1}k_1, \\ P_{z2}(1-P_{z1})k_2 &= P_{z1}k_3. \end{aligned} \tag{6}$$

Equation (5) means that the number of subpopulation states (i.e., the amount of X, Y, and Z in the whole population) is not time-varying in the steady state. In fact, when the system is in its steady state, the degree distribution of nodes with different states is also invariant with time, predicted by the heterogeneous mean-field theory [52]. Combining this point and Eq. (6), we obtain

$$\begin{aligned} \frac{X_k}{Z_k} &= \frac{k_3}{k_1}\frac{P_{z1}}{P_{x2}(1-P_{x1})}, \\ \frac{X_k}{Y_k} &= \frac{P_{y1}}{P_{x2}(1-P_{x1})}, \\ \frac{Y_k}{Z_k} &= \frac{k_3}{k_1}\frac{P_{z1}}{P_{y1}}. \end{aligned} \tag{7}$$

It is interesting that the right-hand sides of Eq. (7) are independent on degree k. From this fact, we can assert that the degree distribution of the nodes in the subpopulation is the same as the degree distribution of underlying interaction network and, surprisingly, the number of nodes with different states is independent on the degree distribution of the interaction network structure in the steady state, which is shown in Appendix A and Fig. 3, respectively.

Finally, considering the detailed balance conditions of edge's state, $\langle\Delta[XY]\rangle = \langle\Delta[XZ]\rangle = \langle\Delta[YZ]\rangle = 0$, we have

$$\begin{aligned} &\sum_{abc}[(a-b)bX_{abc}k_1 - acY_{abc}k_2 + baZ_{abc}k_3] = 0, \\ &\sum_{abc}[-cbX_{abc}k_1 + acY_{abc}k_2 + (c-a)aZ_{abc}k_3] = 0, \\ &\sum_{abc}[cbX_{abc}k_1 + (b-c)cY_{abc}k_2 - baZ_{abc}k_3] = 0. \end{aligned} \tag{8}$$

Then, we can obtain the values of P_{x1}, P_{y1}, and P_{z1} as

$$\begin{aligned} P_{z1} &= \frac{k_2}{k_1+k_2+k_3}\frac{\sum_k kX_k(k-2)}{\sum_k kX_k(k-1)}, \\ P_{x1} &= \frac{\sum_k kX_k}{\sum_k kX_k(k-1)} + \frac{k_2}{k_1+k_2+k_3}\frac{\sum_k kX_k(k-2)}{\sum_k kX_k(k-1)}, \\ P_{y1} &= \frac{k_2}{k_1+k_2+k_3}\frac{\sum_k kX_k(k-2)}{\sum_k kX_k(k-1)}. \end{aligned} \tag{9}$$

Detailed analytical derivations are supplemented in the Appendix B. Combining the relationship of $X_k + Y_k + Z_k = P(k)N$, where $P(k)$ is the degree distribution of the interaction network with Eqs. (7) and (9), we yield the degree distribution of subpopulation with different states as

$$(X_k,\ Y_k,\ Z_k) = \frac{P(k)N}{k_1+k_2+k_3}(k_2,\ k_3,\ k_1),$$

and the fixed point of the whole population as

$$(\rho_x,\ \rho_y,\ \rho_z) = \frac{1}{k_1+k_2+k_3}(k_2,\ k_3,\ k_1), \tag{10}$$

where $\rho_x = \frac{1}{N}\sum_k X_k$ is the proportion of state X subpopulation. Once again, our analytical solutions verify that the degree distribution of the nodes in different subpopulation is the same as that of the static network (see Appendix A), and the fraction of the nodes with different states is independent on the structural properties of the underlying interaction network in the steady state (see Fig. 3). Particularly, it is interesting that this fixed point, indicated by Eq. (10), is consistent with previously reported results in annealed network [6,27,53], and that the number of X-state subpopulation is inversely proportional to both the outflow rate k_1 and the inflow rate k_3, and proportional to the rate k_2 which is indirectly related to state X.

In Fig. 3, the simulation results (scatters) are averaged over 100 independent runs and the analytical solutions of Eq. (10) are shown by wire frame and line. From Fig. 3(a), we can see that the analytical solutions match quite well with those obtained from Monte Carlo simulations in the steady-state region on various networks with different degree distributions. From Fig. 3(b), we can see that there is a large fluctuation

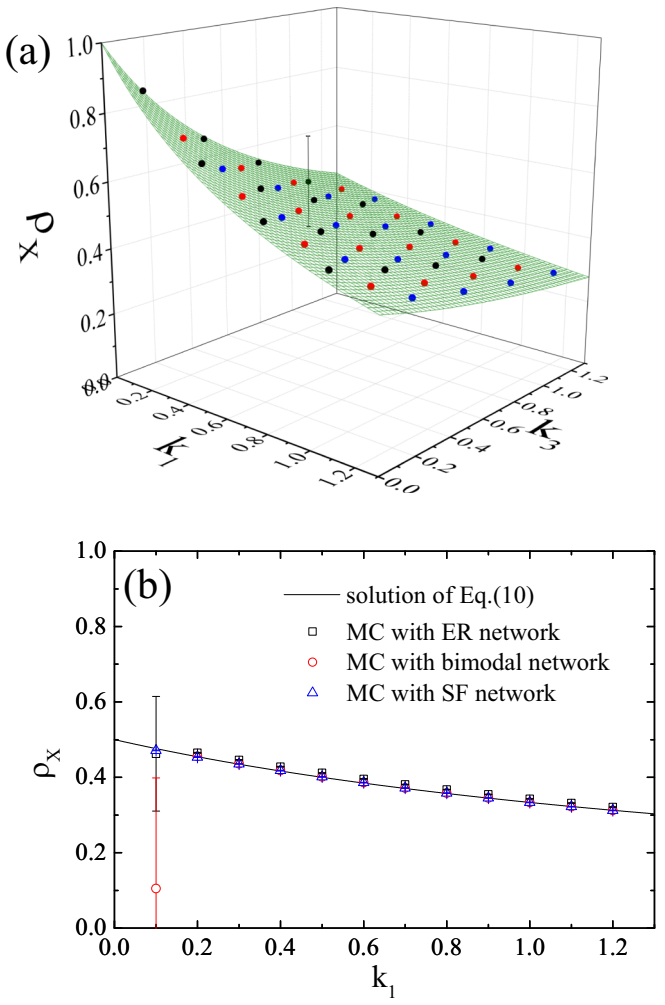

FIG. 3. Comparison of the results obtained by Monte Carlo simulations and by the analytical solutions from Eq. (10) for the cyclic Lotka-Volterra model on static networks with different degree distributions. (a) The proportion of X-state subpopulation ρ_x is plotted as a function of the interaction rate k_1 and the interaction rate k_3. The olive wire frame stands for the analytical solutions, while black, red, and blue circle scatters are simulation results for ER, bimodal, and SF networks, respectively. Parameters: $k_2 = 1.0$. (b) The proportion of X-state subpopulation ρ_x is plotted as a function of the interaction rate k_1. Solid lines are analytical solutions, while square, circle, and triangle scatters are simulation results for ER, bimodal, and SF networks, respectively. Parameters: $k_2 = 1.0$, $k_3 = 1.0$. Simulation results are averaged over 100 independent runs.

and the simulation result is quite below the analytical result at $k_1 = 0.1$ in the bimodal network. For $k_1 = 0.1$, we can calculate the proportion of Z-state subpopulation $\rho_z \approx 0.048$ (very small) from Eq. (10). Because of the value of ρ_z is too small, the system may likely enter into the absorbing state (0, 1, 0), whose possibility is dependent on the network structure. In particular, for our 100 independent runs in the bimodal network with $k_1 = 0.1$, there are about 78 times entering into the absorbing state. Basically, our theoretical solutions for the cyclic Lotka-Volterra dynamic model on static networks match quite well with those obtained from Monte Carlo simulations.

B. The directed migration model

Now, we investigate another model with dynamical symmetry, the simple directed migration model mimicking the migration of animals among three adjacent islands, which does not include neighbor interaction process, as reflected in Fig. 1(c).

In this situation, it is not necessary to define the connectivity probabilities among nodes with different states. We just need one condition, the number and the degree distribution of different subpopulation are invariant with time when the system is in its steady state, to derive the properties of the dynamical system. The stable condition is formulated as $\sum_{k=a+b+c} X_{abc}k_1 = \sum_{k=a+b+c} Z_{abc}k_3 = \sum_{k=a+b+c} Y_{abc}k_2$. From it one can easily obtain

$$\frac{X_k}{Y_k} = \frac{k_2}{k_1}, \quad \frac{X_k}{Z_k} = \frac{k_3}{k_1}, \quad \frac{Y_k}{Z_k} = \frac{k_3}{k_2}, \tag{11}$$

where the right-hand sides of these equations are also independent on the structural properties of the underlying interaction network.

Combine the trivial conservation condition $X_k + Y_k + Z_k = P(k)N$ with Eq. (11), we find that the degree distributions of the nodes in different subpopulation satisfy

$$(X_k,\ Y_k,\ Z_k) = \frac{P(k)N}{\frac{1}{k_1}+\frac{1}{k_2}+\frac{1}{k_3}}\left(\frac{1}{k_1},\ \frac{1}{k_2},\ \frac{1}{k_3}\right),$$

and the fixed point of the whole population is

$$(\rho_x,\ \rho_y,\ \rho_z) = \frac{1}{\frac{1}{k_1}+\frac{1}{k_2}+\frac{1}{k_3}}\left(\frac{1}{k_1},\ \frac{1}{k_2},\ \frac{1}{k_3}\right). \tag{12}$$

From the analytical solutions Eqs. (12) and (10), we find that there are some common grounds between the directed migration model and the cyclic Lotka-Volterra model on static networks. Specifically, in the steady state, the degree distribution of the nodes in different subpopulation is the same as that of the original network of interaction (see Appendix A) and the amount of subpopulation with different states are independent on the structural properties of the underlying network. Nevertheless, in the directed migration model, the number of X-state subpopulation in the stationary state is inversely proportional to the outflow rate k_1, and proportional to the inflow rate k_3 and the rate k_2, in contrast to the case of the cyclic Lotka-Volterra model.

C. The susceptible-infected-recovered-susceptible epidemic model

We next investigate the susceptible-infected-recovered-susceptible epidemic model [13,14] (equivalent to the forest-fire model [40]), which is a dynamical process containing both neighboring interaction and intrinsic transitions, as displayed in Fig. 1(d). In Fig. 4, it is obvious that the numerical solutions of Eqs. (1) and (2) for the time series of nodes with different states are in good agreement with those obtained from computer simulations.

To obtain the analytical solutions, we first consider the condition that the amount of subpopulation with different state and the degree distribution of the nodes in each subpopulation are not time-varying in the steady state, i.e.,

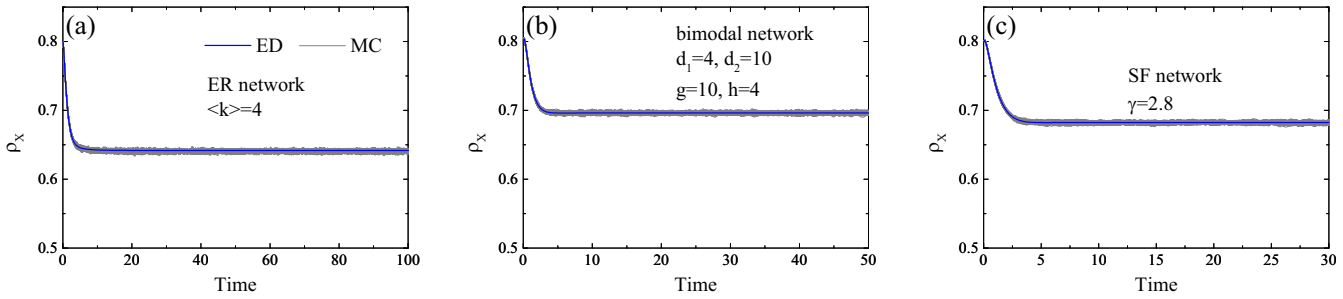

FIG. 4. Comparison of the results obtained by Monte Carlo simulations and by the effective degree approach for the SIRS model on static networks with different degree distributions. The fraction of X-state nodes as a function of the time are explicitly shown for comparison. Thick blue solid lines are the numerical solutions of Eqs. (1) and (2) and thin gray lines are 100 independent runs of simulation results. Parameters: $k_1 = 0.3$, $k_2 = 1.0$, $k_3 = 0.7$.

$\sum_{k=a+b+c} X_{abc}k_1 = \sum_{k=a+b+c} Z_{abc}ak_3 = \sum_{k=a+b+c} Y_{abc}k_2$, and then we can obtain

$$\frac{X_k}{Z_k} = \frac{k_3}{k_1}kP_{z1}, \quad \frac{X_k}{Y_k} = \frac{k_2}{k_1}, \quad \frac{Z_k}{Y_k} = \frac{k_2}{k_3}\frac{1}{kP_{z1}}. \tag{13}$$

From Eq. (13), we find that the degree distribution of the X-state subpopulation is the same as that of the Y-state subpopulation, while they are different from that of the Z-state subpopulation (see Appendix A). Then, if we know the value of P_{z1}, then the above quantities can be solved exactly.

We combine Eqs. (13) and (4), where Eq. (4) is independent of the dynamical processes, to eliminate Y_k and Z_k, and obtain three relationships as

$$\begin{aligned}
\frac{k_1}{k_3} &= \frac{\sum_k kX_k}{\sum_k X_k}(1-P_{x1})(1-P_{x2}),\\
\frac{k_1}{k_2} &= \frac{P_{x2}(1-P_{x1})}{P_{y1}},\\
\frac{k_3}{k_2} &= \frac{\sum_k X_k}{\sum_k kX_k}\frac{P_{z2}(1-P_{z1})}{(1-P_{y1})(1-P_{y2})P_{z1}}.
\end{aligned} \tag{14}$$

To precede, we take into account the detailed balance conditions of edge's state in the steady state, $\langle\Delta[XY]\rangle = \langle\Delta[XZ]\rangle = \langle\Delta[YZ]\rangle = 0$, to obtain the following additional three relationships:

$$\begin{aligned}
&\sum_{abc}[(a-b)X_{abc}k_1 - aY_{abc}k_2 + baZ_{abc}k_3] = 0,\\
&\sum_{abc}[-cX_{abc}k_1 + aY_{abc}k_2 + (c-a)aZ_{abc}k_3] = 0,\\
&\sum_{abc}[cX_{abc}k_1 + (b-c)Y_{abc}k_2 - baZ_{abc}k_3] = 0.
\end{aligned} \tag{15}$$

After further simplifications, we find that P_{z1} has to satisfy the quadratic equation

$$AP_{z1}^2 + BP_{z1} + C = 0, \tag{16}$$

through which one can easily obtain the following self-consistent equation of ρ_k as

$$a_1\rho_k^2 + a_2\rho_k + a_3 = 0. \tag{17}$$

The derivation of Eqs. (16) and (17) are given in Appendix C, and the coefficients A, B, C, a_1, a_2, and a_3 as a function of X_k are as follows:

$$\begin{aligned}
A &= \left[\frac{\sum_k X_k(k-1)}{\sum_k X_k}\left(\frac{k_3}{k_2}+\frac{k_3}{k_1}\right)\right]\sum_k X_k(k-1),\\
B &= \left[3+\frac{k_3+k_1}{k_2}+\frac{k_2}{k_1}-\frac{k_3}{k_1}\frac{\sum_k X_k(k-1)}{\sum_k X_k}\right]\sum_k X_k(k-1),\\
C &= \left[\frac{\sum_k X_k}{\sum_k X_k(k-1)}\frac{k_1+k_2+k_3}{k_3}-\frac{k_2+k_1}{k_1}\right]\sum_k X_k(k-1),\\
a_1 &= A\left(\frac{k_1}{k_3k}\right)^2 - B\frac{k_1}{k_3k}\left(1+\frac{k_1}{k_2}\right)+C\left(1+\frac{k_1}{k_2}\right)^2,\\
a_2 &= B\frac{k_1}{k_3k} - 2C\left(1+\frac{k_1}{k_2}\right),\\
a_3 &= C.
\end{aligned}$$

The convergence problem of nonlinear equations with k dimensions in Eqs. (17) is difficult for us to obtain exact solutions. Fortunately, we can use an invariant to reduce the dimensions from k to one. Now we calculate the fraction of X-state subpopulation ρ_x in the steady state as follows: (i) Denote the parameter $z = \frac{\sum_k X_k}{\sum_k X_k(k-1)}$; (ii) Give any $z \in (0, 1]$, we calculate the ρ_k by Eqs. (17) and get a new z'; (iii) Compare the absolute value of $z' - z$, the value zero of $z' - z$ is the solution. In Fig. 5, the simulation results which are shown by scatters are averaged over 100 independent runs and the analytical solutions of Eq. (17) are denoted by wire frame and line. It is obvious that the results from the analytical solution match quite well with those obtained from Monte Carlo simulations for the SIRS epidemic model on various static networks with different degree distributions.

In annealed networks, the steady-state solution of the SIRS model can be exactly mapped to that of the SIS model by rescaling the density of infected individuals (X-state nodes) with the immunity decay rate (the interaction rate k_2) [54], and all the critical properties of the SIRS model are the same as the SIS model (independent on k_2) [40]. However, on static networks, the steady-state solution of the SIRS model, i.e., Eq. (17), is more complicated than that of the SIS model in Ref. [47], and we will show below that the threshold curve is not independent on the interaction rate k_2.

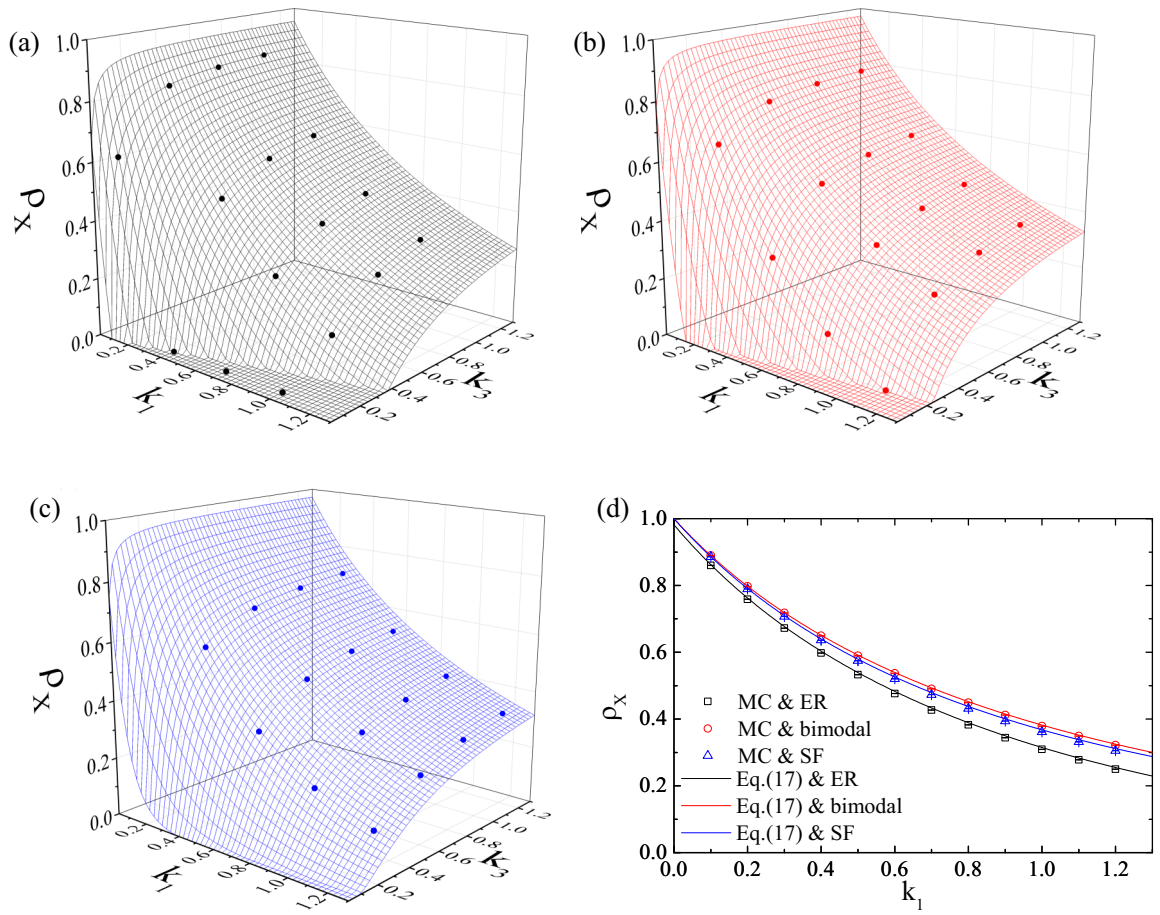

FIG. 5. Comparison of the results obtained by Monte Carlo simulations and by the analytical solutions from Eq. (17) for the SIRS model on static networks with different degree distributions. (a–c) The proportion of X-state subpopulation ρ_x is plotted as a function of the interaction rate k_1 and the interaction rate k_3. The wire frame stands for the analytical solutions, while circle scatters are simulation results. Parameters: (a) ER network, (b) bimodal network, (c) SF network, (a–c) $k_2 = 1.0$. (d) The proportion of X-state subpopulation ρ_x is plotted as a function of the interaction rate k_1. Solid lines are analytical solutions, while square, circle, and triangle scatters are simulation results for ER, bimodal, and SF networks, respectively. Parameters: $k_2 = 1.0$, $k_3 = 1.0$. Simulation results are averaged over 100 independent runs.

The root $\rho_k = X_k/N_k = 0$ corresponds to the case of all Z-state nodes in the network, which is the absorbing state (0, 0, 1) and always a solution. A stationary solution for the coexistence of all the X, Y, and Z states in the system is obtained when P_{z1} has a nontrivial solution in the interval $0 < P_{z1} \leqslant 1$. We denote the left-hand side of Eq. (23) by $f(P_{z1})$. It is easy to see that $P_{z1} = 0$ is a trivial solution of Eq. (16). Hence, it is easy to realize that, on uncorrelated static random networks, the threshold curve surface for the coexistence of all states, i.e., indicated by solving $\frac{d[f(P_{z1})]}{dP_{z1}}|_{P_{z1}=0} = 0$, is given by

$$\frac{\langle k\rangle}{\langle k^2\rangle - \langle k\rangle} = \frac{k_3(k_1+k_2)}{k_1(k_1+k_2+k_3)}. \tag{18}$$

It is clear that the threshold curve surface Eq. (18) is not independent on the interaction rate k_2 on static networks, while it does depend on the interaction rate k_2 on annealed networks [54]. Remarkably, our results also verify the previous results of some special cases. For instance, in the case of random regular network [55], $P(k) = \delta(k - k_0)$, the solution of Eq. (18) reads as $\lambda(\gamma) = \frac{1+\gamma}{k-2+\gamma(k-1)}$, which is consistent with the result in Ref. [14]. What is more, as the interaction rate $k_2 \to \infty$, the SIRS epidemic model degenerates into the SIS epidemic model, and the solution of Eq. (18) can be rewritten as $\lambda = \frac{\langle k\rangle}{\langle k^2\rangle - \langle k\rangle}$, which is consistent with the result in Refs. [47,56]. Besides, as the interaction rate $k_2 = 0$, the SIRS epidemic model will degenerates into the classical SIR epidemic model, for which the solution of Eq. (18) is $\lambda = \frac{\langle k\rangle}{\langle k^2\rangle - 2\langle k\rangle}$, consistent with the finding in Refs. [44,54]. (Note that here we have used $\lambda = k_3/k_1$ and $\gamma = k_2/k_1$ for a clear comparison with previously obtained results in Refs. [14,44,47,54,56]).

We use the quasistationary method introduced in Ref. [57], which permits to overcome the difficulties in simulating finite size systems with absorbing states, to simulation the threshold of phase transition on static networks. In Fig. 6, we plot the threshold curves for fixed $k_2 = 1.0$ against network size N and show that, with the increase of the size of ER random networks, the threshold curves estimated by the quasistationary simulation [58,59] move closer and closer to the theoretical values predicted by Eq. (18).

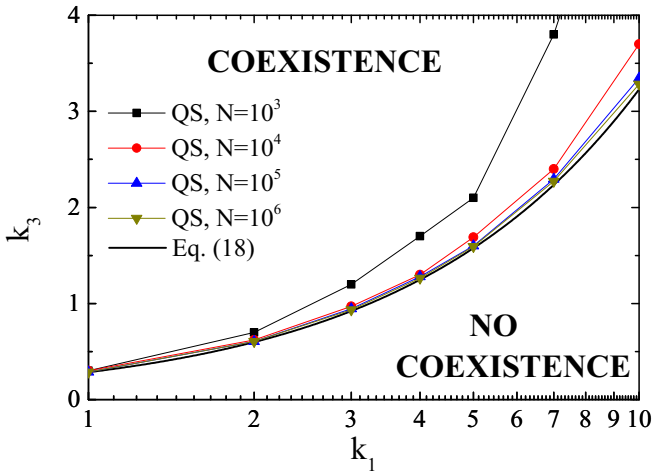

FIG. 6. Phase diagram of the SIRS model on ER random networks with different network size N and $\langle k\rangle = 4$. The coexistence phase of X-Y-Z and the no-coexistence phase are separated by the threshold curves from the quasi-stationary simulation method (scatters with line to guide the eye) and the analytical solutions of Eq. (18) as $k_3 = \frac{k_1(k_1+1)}{3k_1+4}$ (thick solid line). Parameters: $k_2 = 1.0$.

D. The predator-prey with empty sites model

In the last case, we investigate another model with dynamical asymmetry, the predator-prey with empty sites model [10,41], which include one intrinsic transition process and two neighboring interaction processes, as illustrated in Fig. 1(e). In Fig. 7, it is shown that the numerical solutions of Eqs. (1) and (2) for the time series of the fraction of subpopulation are in good agreement with those obtained from computer simulations.

In a similar way as in the analysis of the above three-state models, considering the number of and the degree distribution the nodes in each subpopulation are not time-varying in the steady state, we have

$$\begin{aligned}\frac{X_k}{Z_k} &= \frac{k_3}{k_1}kP_{z1},\\ \frac{X_k}{Y_k} &= \frac{k_2}{k_1}k(1-P_{y1})(1-P_{y2}),\\ \frac{Y_k}{Z_k} &= \frac{k_3}{k_2}\frac{P_{z1}}{(1-P_{y1})(1-P_{y2})}.\end{aligned} \tag{19}$$

From Eq. (19), we can find that the degree distribution of the Y-state subpopulation is the same as that of the Z-state subpopulation, while they are different from that of the X-state subpopulation (see Appendix A). We combine Eqs. (19) and (4) to eliminate Y_k and Z_k, and obtain the following equations

$$\begin{aligned}\frac{k_1}{k_3} &= \frac{\sum_k kX_k}{\sum_k X_k}(1-P_{x1})(1-P_{x2}),\\ \frac{k_1}{k_2} &= \frac{\sum_k kX_k}{\sum_k X_k}\frac{(1-P_{y1})(1-P_{y2})(1-P_{x1})P_{x2}}{P_{y1}},\\ \frac{k_3}{k_2} &= \frac{P_{z2}(1-P_{z1})}{P_{z1}}.\end{aligned} \tag{20}$$

As before, considering the detailed balance condition of edge's state in the steady state, $\langle\Delta[XY]\rangle = \langle\Delta[XZ]\rangle = \langle\Delta[YZ]\rangle = 0$, we obtain additional three relationships as

$$\begin{aligned}&\sum_{abc}[(a-b)X_{abc}k_1 - acY_{abc}k_2 + baZ_{abc}k_3] = 0,\\ &\sum_{abc}[-cX_{abc}k_1 + acY_{abc}k_2 + (c-a)aZ_{abc}k_3] = 0,\\ &\sum_{abc}[cX_{abc}k_1 + (b-c)cY_{abc}k_2 - baZ_{abc}k_3] = 0.\end{aligned} \tag{21}$$

After further simplifications, we find that P_{z1} has to satisfy the quadratic equation

$$A'P_{z1}^2 + B'P_{z1} + C' = 0. \tag{22}$$

By using the auxiliary parameter $z = \frac{\sum_k X_k}{\sum_k X_k(k-1)}$, the coefficients A', B', and C' as a function of X_k can be given as follows:

$$\begin{aligned}A' &= \left[\left(1+\frac{k_3}{k_2}\right)\frac{1}{z}\right]\sum_k X_k,\\ B' &= \left[-\left(2+\frac{k_3}{k_2}\right)\frac{1}{z} + 1 + \frac{k_1}{k_3}\left(1+\frac{k_3}{k_2}\right)\right.\\ &\quad \left.-\frac{k_1}{k_2}\left(2+\frac{k_3}{k_2}\right)\right]\sum_k X_k,\\ C' &= \left\{z\left[\frac{k_1}{k_3} - \frac{k_1}{k_2}\left(1+\frac{k_1}{k_3}\right)\right] + \frac{1}{z} - \left(1+\frac{k_1}{k_3}-\frac{k_1}{k_2}\right)\right\}\sum_k X_k.\end{aligned}$$

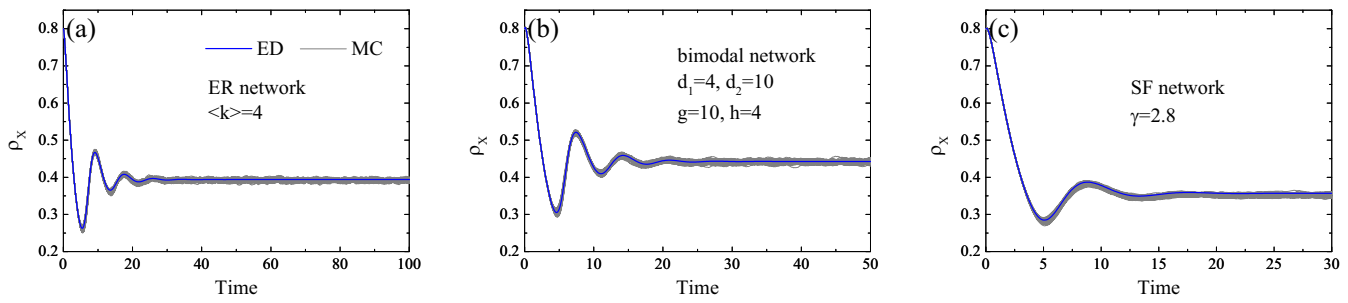

FIG. 7. Comparison of the results obtained by Monte Carlo simulations and by the effective degree approach for the predator-prey with empty sites model on static networks with different degree distributions. The fraction of X-state nodes as a function of the time are explicitly shown for comparison. Thick blue solid lines are the numerical solutions of Eqs. (1) and (2) and thin gray lines are 100 independent runs of simulation results. Parameters: $k_1 = 0.3$, $k_2 = 1.0$, $k_3 = 0.7$.

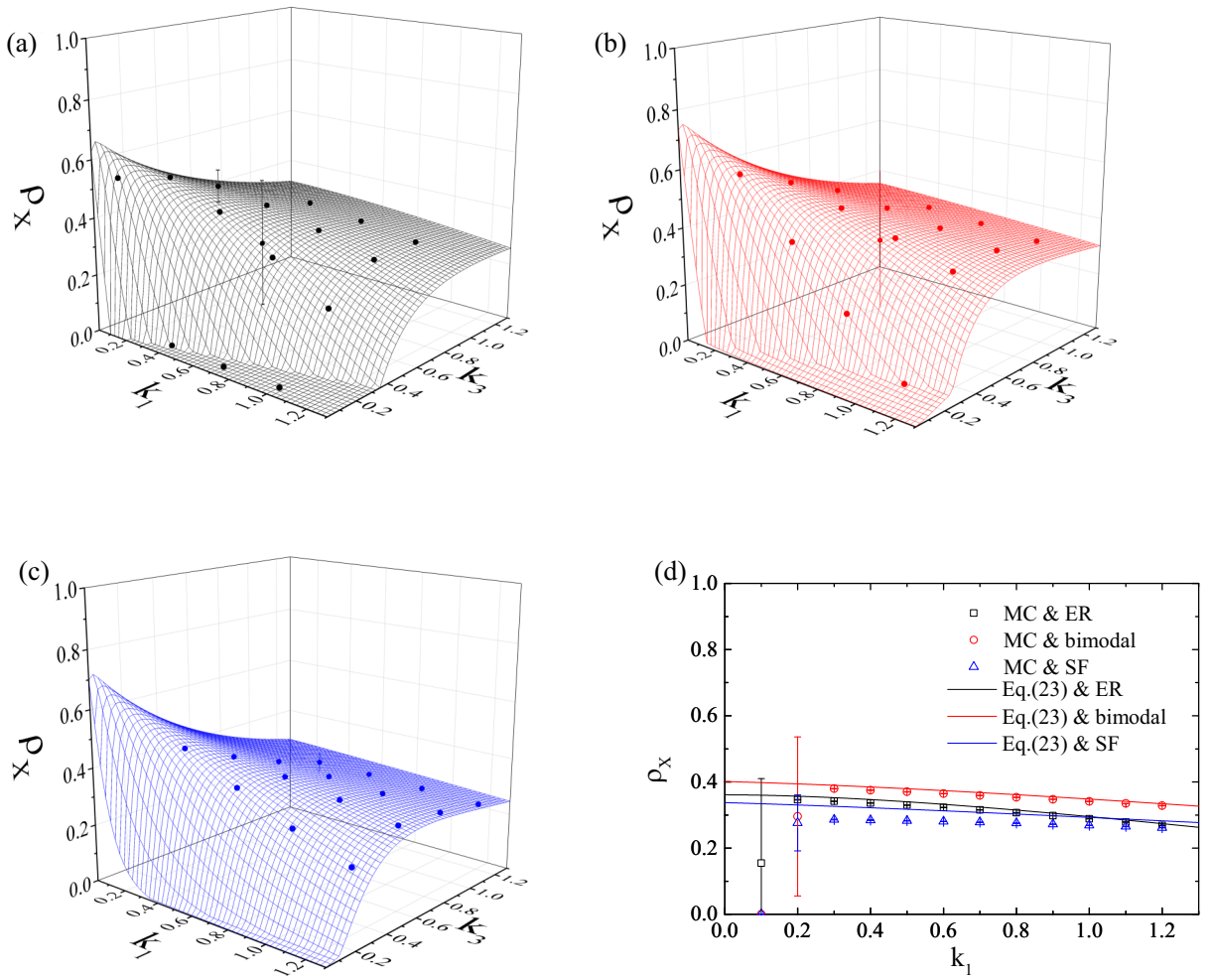

FIG. 8. Comparison of the results obtained by Monte Carlo simulations and by the analytical solutions from Eq. (23) for the predator-prey with empty sites model on static networks with different degree distributions. (a–c) The proportion of X-state subpopulation ρ_x is plotted as a function of the interaction rate k_1 and the interaction rate k_3. The wire frame stands for the analytical solutions, while circle scatters are simulation results. Parameters: (a) ER network, (b) bimodal network, (c) SF network, (a–c) $k_2 = 1.0$. (d) The proportion of X-state subpopulation ρ_x is plotted as a function of the interaction rate k_1. Solid lines are analytical solutions, while square, circle, and triangle scatters are simulation results for ER, bimodal, and SF networks, respectively. Parameters: $k_2 = 1.0$, $k_3 = 1.0$. Simulation results are averaged over 100 independent runs.

From Eq. (22), we yield the following self-consistent equations of ρ_k:

$$a_1'\rho_k^2 + a_2'\rho_k + a_3' = 0. \tag{23}$$

Where the coefficients a_1', a_2', and a_3' can be given as follows:

$$\begin{aligned}
a_1' = {} & A'\left[C'zk + \frac{k_1}{k_3}(1-z)\right]^2 + \left[k(1-z) - \frac{k_1}{k_3} + B'kz\right] \\
& \times\left[(1-z)\left(C'k - \frac{k_1}{k_3}B'\right) - \frac{k_1}{k_3}C'\right], \\
a_2' = {} & -2A'C'zk\left[C'zk + \frac{k_1}{k_3}(1-z)\right] \\
& + (1-z)[k(1-z) + B'kz]\left[\frac{k_1}{k_3}B' - 2C'k\right] \\
& + \frac{k_1}{k_3}C'k[2 + (B'-2)z], \\
a_3' = {} & A'(C'zk)^2 + C'k(1-z)[k(1-z) + B'kz].
\end{aligned}$$

We calculate the fraction of X-state subpopulation ρ_x in the steady state as follows: (i) Give any $z \in (0, 1]$, we calculate the ρ_k by Eqs. (23) and get a new z'; (ii) Compare the absolute value of $z' - z$, the value zero of $z' - z$ is the solution. The results are summarized in Fig. 8.

In a similar way as in the analysis of the SIRS model, we denote the left-hand side of Eq. (22) by $h(P_{z1})$. Considering the equality $\frac{d[h(P_{z1})]}{dP_{z1}}|_{P_{z1}=0} = 0$, we are able to find the threshold curve surface for the coexistence of all three states in the predator-prey with empty sites model for uncorrelated static random networks:

$$\begin{aligned}
& 1 + \left[\frac{k_1}{k_3} - \frac{k_1}{k_2}\left(1 + \frac{k_1}{k_3}\right)\right]\left(\frac{\langle k\rangle}{\langle k^2\rangle - \langle k\rangle}\right)^2 \\
& -\left(1 + \frac{k_1}{k_3} - \frac{k_1}{k_2}\right)\frac{\langle k\rangle}{\langle k^2\rangle - \langle k\rangle} = 0.
\end{aligned} \tag{24}$$

In Fig. 8, the simulation results which are displayed by scatters are averaged over 100 independent runs and the

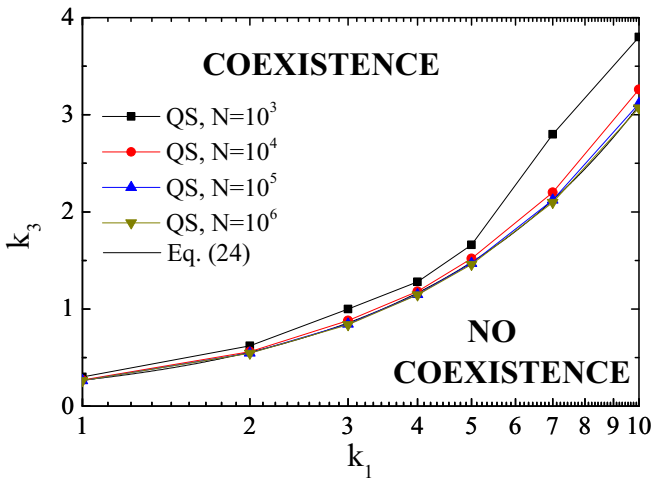

FIG. 9. Phase diagram of the predator-prey with empty sites model on static ER random networks with different network size N and $\langle k\rangle = 4$. The coexistence phase of X-Y-Z and the no-coexistence phase are separated by the threshold curves from the quasi-stationary simulation method (scatters with line to guide the eye) and the analytical solutions of Eq. (24) as $k_3 = \frac{k_1(k_1+3)}{3(k_1+4)}$ (thick solid line). Parameters: $k_2 = 1.0$.

analytical solutions of Eq. (23) are denoted by wire frame and line. We can see that, in bimodal and ER random networks, the results from the analytical solution match well with those obtained from Monte Carlo simulations for the predator-prey with empty sites model. However, in SF random networks, a visible discrepancy of ρ_x between the simulations and analytical solutions can be observed.

The reason is attributed to the extent of accuracy the ED approximate method Eq. (3), which just considers the dynamic correlation between the nearest neighbors, whose accuracy will decrease in the heterogeneous networks. In Fig. 9, we plot the threshold curve for fixed $k_2 = 1.0$ against network size N of ER random networks, and we can see that the accuracy of the threshold curves of our method matches quite well with the results from the quasi-stationary simulations. We believe that the accuracy of effective degree approach for the prediction of the fraction of different states in the steady state and the threshold curved surface will be promoted further by taken into consideration of higher-order dynamic correlation in SF random networks.

V. CONCLUSION AND DISCUSSION

In summary, with the aid of the effective degree approximation method we have addressed the dynamic correlation problem of nearest neighbors' states of typical three-state dynamical processes unfolding on static networks, including the cyclic Lotka-Volterra dynamics, the directed migration dynamics, the forest-fire (or SIRS) dynamics, and the predator-prey with empty sites dynamics. We focused mainly on the relaxation behavior as well as the extinction threshold of different states in the system. By analyzing the coupled ordinary differential equations and employing the statistical properties of the systems in the steady state, we are able to obtain explicitly the analytical solutions for the four typical dynamics.

Particularly, the threshold curved surface for each three-state dynamical model can be calculated as a corollary of the propagation sizes of the states. In the cyclic Lotka-Volterra model, we found that the macroscopic behaviors on static networks are the same as those on annealed networks, including: (1) The fraction of all the three states will oscillate damply to a fixed point both on static and annealed networks with identical degree distribution; (2) The solution of the fixed point is identical between static network and annealed network; (3) There are no phase transition for the cyclic Lotka-Volterra dynamical process on both static and annealed networks. For the directed migration model (in which the three states are of rotational symmetry as in the case of cyclic Lotka-Volterra model), we also found that the macroscopic behaviors on static networks are the same as those on annealed networks. We therefore speculate that dynamical symmetry plays an important role against the consistency between the outcomes of dynamical processes taking place on static and annealed networks.

In asymmetric dynamical model, i.e., the SIRS epidemic model and the predator-prey with empty sites model, we derived the self-consistent equations of the fraction of different states in the steady state and the threshold curved surface, and found that the results on static networks are more complicated than those on their annealed counterparts. For the SIRS epidemic model, there are some important differences between the outcomes of the dynamical process carried out on static networks and annealed networks, including: (1) The steady-state solution of the SIRS model on static networks cannot be mapped to that of the SIS model by rescaling the density of infected individuals (state X nodes) with the immunity decay rate (the interaction rate k_2); (2) the threshold curve surface is not independent on the interaction rate k_2, specifying the rate of recovered individuals getting back to susceptible ones.

It is worth pointing out that, for all the time series of the propagating size, the steady-state solution of the propagating size, or the threshold curve surface, the results forecasted by our theoretical analysis are in good agreement with those by Monte Carlo simulations, expect for the case of heterogeneous networks. However, we believe that the accuracy of propagating size and threshold of the three-state model on static, heterogeneous network of interaction can be further promoted by taken into account higher-order dynamic correlation.

For equilibrium three-state dynamics, our theoretical analysis captures essential elements on degree-uncorrelated static networks (not arbitrary network structure) with arbitrary degree distributions. And our analysis will provide meaningful guidance for future researches. On one hand, dynamical processes on degree-correlated networks, directed networks, weighted networks, and activity-driven networks can be considered to approximate the dynamics of real complex systems. On the other hand, our approach can also be conveniently extended to nonequilibrium dynamical models on networks, such as three-state oscillators [60,61] and driven Potts models [62] where the state of each node is similarly dependent on its neighbors.

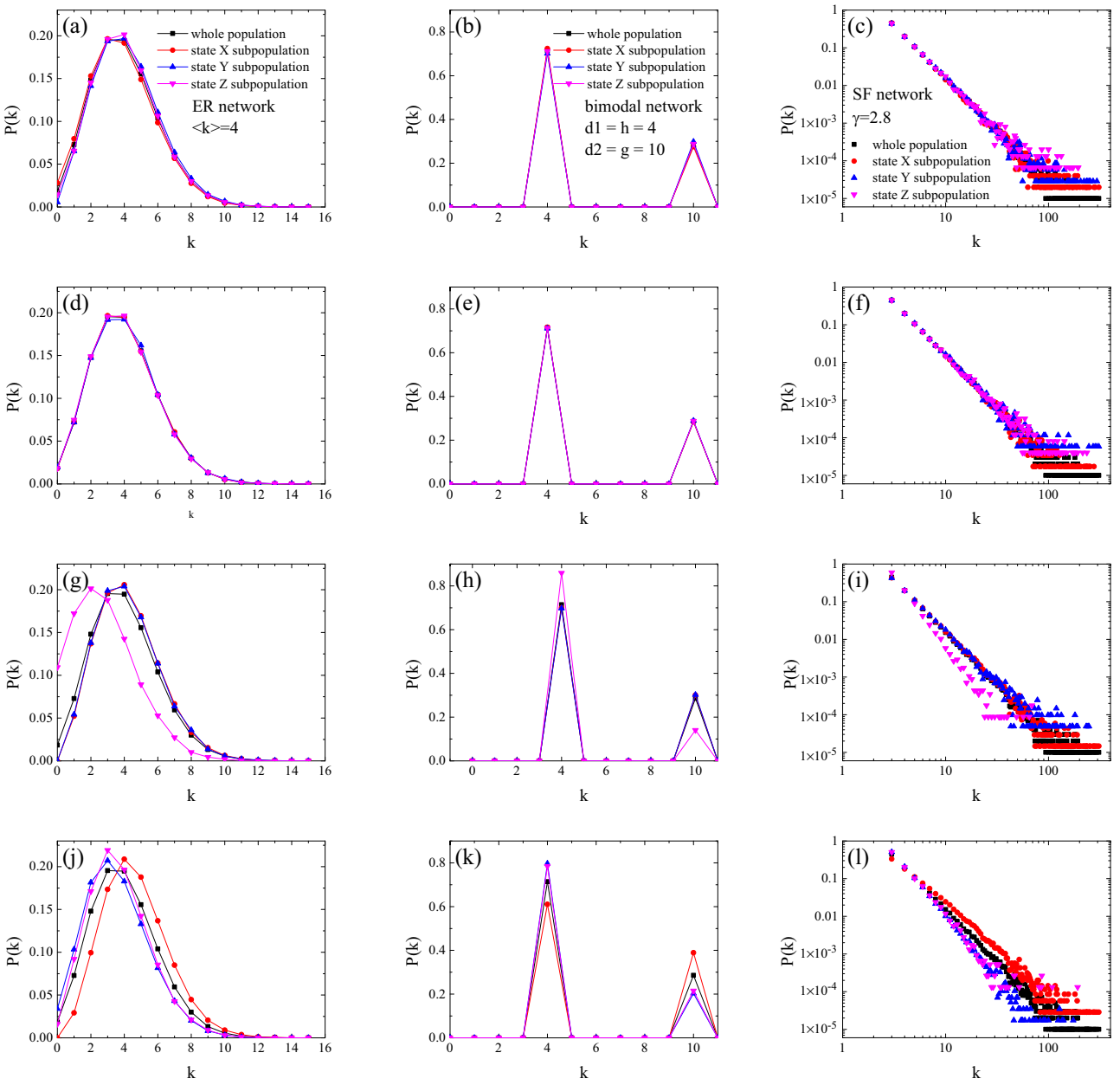

FIG. 10. The degree distributions of different subpopulations obtained by one Monte Carlo simulation for the four kinds of models on static networks with different degree distributions at time $t = 200$ for comparison. Parameters: the top three panels are for the cyclic Lotka-Volterra model, the second row panels are for the directed migration model, the third row panels are for the SIRS model, and the bottom three panels are for the predator-prey with empty sites model; the left column panels are for ER networks with average degree $\langle k \rangle = 4$, the middle column panels are for bimodal networks with $d_1 = h = 4$ and $d_2 = g = 10$, and the right column panels are for SF networks with the power exponent $\gamma = 2.8$. The interaction rates are $k_1 = 0.3$, $k_2 = 1.0$, and $k_3 = 0.7$, respectively.

ACKNOWLEDGMENTS

This work was supported by the National Natural Science Foundation of China (Grants No. 11705147 and No. 11975111).

APPENDIX A: DEGREE DISTRIBUTION OF THE NODES AMONG DIFFERENT SUBPOPULATIONS

In this section, we measure the degree distribution of the nodes in different subpopulations and also in the whole population for the four kinds of dynamical models on typical complex networks.

From Figs. 10(a)–10(f), we can see that, for the cyclic Lotka-Volterra model and the directed migration model, the degree distribution of the nodes in different subpopulation in the steady state are the same as that of the underlying network of interaction. From Figs. 10(g)–10(i), we can see that, for the forest-fire dynamical model, the degree distribution of X-state subpopulation is the same as that of Y-state subpopulation, approximately equal to that of the original network,

and different from Z-state subpopulation in the steady state. From Figs. 10(j)–10(l), we can see that, for the predator-prey with empty sites model, the degree distribution of X-state subpopulation in the steady state is different from that of Y-state subpopulation, that of Z-state subpopulation, and that of the original network, while the degree distribution of Y-state subpopulation is the same as that of Z-state subpopulation in the steady state.

APPENDIX B: DERIVATION OF EQUATION (9)

Here, we show detailed derivations to obtain Eq. (9). First, using the relationships of $\sum_i \binom{j}{i} P^i(1-P)^{j-i} i = jP$ and $\sum_i \binom{j}{i} P^i(1-P)^{j-i} i^2 = j(j-1)P^2 + jP$, we get

$$\sum_k \sum_{k=a+b+c} cY_{abc} k_2(-c+b) = \sum_k k_2 Y_k (1-P_{y2}) k (P_{y1}-1)[2P_{y2}(k-1)(P_{y1}-1) - (k-1)P_{y1} + k].$$

And then, combining the relationships of $(1-P_{y1})(1-P_{y2})k_2 = P_{y1}k_1$ in Eq. (6) and $\frac{X_k}{Y_k} = \frac{P_{y1}}{P_{x2}(1-P_{x1})}$ in Eq. (7), we obtain

$$\sum_k \sum_{k=a+b+c} cY_{abc} k_2(-c+b) = \sum_k k_1 X_k P_{x2}(P_{x1}-1) k \left[(k-1)\left(1 + \frac{2k_1}{k_2}\right) P_{y1} + (2-k) \right].$$

After doing some algebra, Eq. (8) can be rewritten as a set of linear equations,

$$\sum_k k X_k [(1+P_{x2})(k-1)P_{x1} - (kP_{x2} - P_{x2} + 1) - (k-1)P_{y1} + (k-1)P_{z1}k_3/k_2] = 0,$$

$$\sum_k k X_k [(P_{x2}-1)(1-P_{x1})(k-1) + (k-1)P_{y1} + (k-2) - P_{z1}(k-1)(2+k_3/k_2)] = 0,$$

$$\sum_k k X_k [(1-P_{x2})(k-1)(1-P_{x1}) - (k-1)P_{z1}k_3/k_2 + (k-2) - P_{y1}(k-1)(1+2k_1/k_2)] = 0,$$

with the augmented matrix,

$$\begin{bmatrix} (1+P_{x2})Q_2 & -Q_2 & \frac{k_3}{k_2}Q_2 & Q_1 + P_{x2}Q_2 \\ (1-P_{x2})Q_2 & Q_2 & -\left(2+\frac{k_3}{k_2}\right)Q_2 & Q_1 - P_{x2}Q_2 \\ (P_{x2}-1)Q_2 & -\left(1+2\frac{k_1}{k_2}\right)Q_2 & -\frac{k_3}{k_2}Q_2 & Q_1 - (2-P_{x2})Q_2 \end{bmatrix},$$

where $Q_1 = \sum_k kX_k$, $Q_2 = \sum_k k(k-1)X_k$, and $P_{x2} = k_3/(k_1+k_3)$ in Eq. (6). Then, we can obtain the Eq. (9) easily.

APPENDIX C: DERIVATION OF EQUATIONS (16) AND (17)

Here, we give detailed derivations to yield Eqs. (16) and (17). Substituting Eq. (13) into Eq. (15), then we get the following equations after rearrangement:

$$\sum_k X_k [k(P_{x1} + P_{x1}P_{x2} - P_{x2}) - kP_{y1} + (k-1)P_{z2}(1-P_{z1})] = 0, \tag{C1}$$

$$\sum_k X_k \{[(k-1)(P_{z2}-1)(P_{z1}-1) - (k-1)P_{z1} - 1] - k(1-P_{x1})(1-P_{x2}) + kP_{y1}\} = 0, \tag{C2}$$

$$\sum_k X_k \{k(1-P_{x1})(1-P_{x2}) - k(2P_{y2}-1)(1-P_{y1}) - (k-1)P_{z2}(1-P_{z1})\} = 0. \tag{C3}$$

After doing some algebra, we obtain

$$\sum_k X_k (kP_{x1} - 1) = \sum_k X_k (k-1)P_{z1}, \tag{C4}$$

$$P_{x2}(P_{x1}-1) = P_{y2}(P_{y1}-1), \tag{C5}$$

$$P_{x2} = \frac{k_1}{k_3} \frac{\sum_k X_k}{\sum_k X_k (k-1)(P_{z1}-1)} + 1, \tag{C6}$$

$$\frac{k_1}{k_2} P_{y1} = P_{x2}(1-P_{x1}), \tag{C7}$$

$$P_{y1} = \frac{k_2}{k_1} \frac{\sum_k X_k (k-1)(1-P_{z1})}{\sum_k X_k k} - \frac{k_2}{k_3} \frac{\sum_k X_k}{\sum_k X_k k}, \tag{C8}$$

$$P_{z2}(1-P_{z1}) = \frac{k_3}{k_2} \frac{\sum_k kX_k}{\sum_k X_k} P_{z1}(1-P_{y1})(1-P_{y2}), \tag{C9}$$

where Eqs. (C4)–(C9) are obtained by Eq. (C1) plus Eq. (C2), Eq. (C1) plus Eq. (C3), substituting Eq. (C4) into the first formula of Eq. (14), the second formula of Eq. (14), substituting Eq. (C4) and (C6) into the second formula of Eq. (14), and the third formula of Eq. (14), respectively.

Finally, substituting Eqs. (C4)–(C9) into Eq. (C1), we can obtain Eq. (16) with the following coefficients:

$$\begin{aligned} A &= \left[\frac{\sum_k X_k(k-1)}{\sum_k X_k}\left(\frac{k_3}{k_2}+\frac{k_3}{k_1}\right)\right]\sum_k X_k(k-1), \\ B &= \left[3+\frac{k_3+k_1}{k_2}+\frac{k_2}{k_1}-\frac{k_3}{k_1}\frac{\sum_k X_k(k-1)}{\sum_k X_k}\right]\sum_k X_k(k-1), \\ C &= \left[\frac{\sum_k X_k}{\sum_k X_k(k-1)}\frac{k_1+k_2+k_3}{k_3}-\frac{k_2+k_1}{k_1}\right]\sum_k X_k(k-1). \end{aligned} \tag{C10}$$

According to the relationship of $k_1X_k = P_{z1}k_3k(N_k - X_k - \frac{k_1}{k_2}X_k)$, which is from Eq. (13), we can obtain Eq. (17) with the following coefficients:

$$\begin{aligned} a_1 &= A\left(\frac{k_1}{k_3k}\right)^2 - B\frac{k_1}{k_3k}\left(1+\frac{k_1}{k_2}\right)+C\left(1+\frac{k_1}{k_2}\right)^2, \\ a_2 &= B\frac{k_1}{k_3k}-2C\left(1+\frac{k_1}{k_2}\right), \\ a_3 &= C, \end{aligned} \tag{C11}$$

where A, B, and C are from Eq. (C10).

[1] S. J. Maynard, *Models in Ecology* (Cambridge University Press, Cambridge, 1974).
[2] R. M. May, *Stability and Complexity in Model Ecosystems* (Princeton University Press, Princeton, 2001).
[3] D. Ulrich, M. Mauro, P. Michel, and C. T. Uwe, J. Phys. A: Math. Theor. **51**, 063001 (2018).
[4] J. Hofbauer and K. Sigmund, *Eolutionary Games and Population Dynamics* (Cambridge University Press, Cambridge, 1998).
[5] D. Neal, *Introduction to Population Biology* (Cambridge University Press, Cambridge, 2004).
[6] T. Reichenbach, M. Mobilia, and E. Frey, Phys. Rev. E **74**, 051907 (2006).
[7] M. Berr, T. Reichenbach, M. Schottenloher, and E. Frey, Phys. Rev. Lett. **102**, 048102 (2009).
[8] S. Chen and U. C. Täuber, Phys. Biol. **13**, 025005 (2016).
[9] P. P. Avelino, D. Bazeia, L. Losano, J. Menezes, and B. F. de Oliveira, Europhys. Lett. **121**, 48003 (2018).
[10] M. Mobilia, I. T. Georgiev, and U. C. Täuber, Phys. Rev. E **73**, 040903(R) (2006).
[11] J. Zhao and M. Wang, Nonlin. Anal. Real **16**, 250 (2014).
[12] U. C. Täuber, J. Phys. A: Math. Theor. **45**, 405002 (2012).
[13] M. Kuperman and G. Abramson, Phys. Rev. Lett. **86**, 2909 (2001).
[14] J. Joo and J. L. Lebowitz, Phys. Rev. E **70**, 036114 (2004).
[15] Z. Wang, B. Xu, and H.-J. Zhou, Sci. Rep. **4**, 5830 (2014).
[16] J. Menezes, B. Moura, and T. A. Pereira, Europhys. Lett. **126**, 18003 (2019).
[17] S. Clar, B. Drossel, and F. Schwabl, J. Phys. Condens. Mat. **8**, 6803 (1996).
[18] Z. Zheng, W. Huang, S. Li, and Y. Zeng, Ecol. Model. **348**, 33 (2017).
[19] B. Kerr, M. A. Riley, M. W. Feldman, and B. J. M. Bohannan, Nature **418**, 171 (2002).
[20] B. C. Kirkup and M. A. Riley, Nature **428**, 412 (2004).
[21] J. B. C. Jackson and L. Buss, Proc. Natl. Acad. Sci. USA **72**, 5160 (1975).
[22] B. Sinervo and C. M. Lively, Nature **380**, 240 (1996).
[23] D. Lee, B. P. McGreevy, and D. J. Barraclough, Cogn. Brain Res. **25**, 416 (2005).
[24] T. Reichenbach, M. Mobilia, and E. Frey, Nature **448**, 1046 (2007).
[25] A. Dobrinevski and E. Frey, Phys. Rev. E **85**, 051903 (2012).
[26] J. Knebel, T. Krüger, M. F. Weber, and E. Frey, Phys. Rev. Lett. **110**, 168106 (2013).
[27] R. West, M. Mobilia, and A. M. Rucklidge, Phys. Rev. E **97**, 022406 (2018).
[28] E. Valdano, L. Ferreri, C. Poletto, and V. Colizza, Phys. Rev. X **5**, 021005 (2015).
[29] D. Soriano-Paños, L. Lotero, A. Arenas, and J. Gómez-Gardeñes, Phys. Rev. X **8**, 031039 (2018).
[30] E. Valdano, M. R. Fiorentin, C. Poletto, and V. Colizza, Phys. Rev. Lett. **120**, 068302 (2018).
[31] J. Hindes and I. B. Schwartz, Phys. Rev. Lett. **117**, 028302 (2016).
[32] S. Galam, Y. G. (Feigenblat), and Y. Shapir, J. Math. Sociol. **9**, 1 (1982).
[33] S. N. Dorogovtsev, A. V. Goltsev, and J. F. F. Mendes, Phys. Rev. E **66**, 016104 (2002).
[34] F. Y. Wu, Rev. Mod. Phys. **54**, 235 (1982).
[35] F. Graner and J. A. Glazier, Phys. Rev. Lett. **69**, 2013 (1992).
[36] M. Ifti and B. Bergersen, Eur. Phys. J. B **37**, 101 (2004).

[37] S. Pigolotti, C. López, and E. Hernández-García, Phys. Rev. Lett. **98**, 258101 (2007).
[38] G. Szabó and T. Czárán, Phys. Rev. E **63**, 061904 (2001).
[39] B. J. Worton, Ecol. Model. **38**, 277 (1987).
[40] J.-D. Bancal and R. Pastor-Satorras, Eur. Phys. J. B **76**, 109 (2010).
[41] A. J. McKane and T. J. Newman, Phys. Rev. Lett. **94**, 218102 (2005).
[42] M. Catanzaro, M. Boguñá, and R. Pastor-Satorras, Phys. Rev. E **71**, 027103 (2005).
[43] G. E. Allen and C. Dytham, Biosystems **98**, 37 (2009).
[44] J. Lindquist, J. Ma, P. van den Driessche, and F. H. Willeboordse, J. Math. Biol. **62**, 143 (2011).
[45] C.-R. Cai, Z.-X. Wu, and J.-Y. Guan, Phys. Rev. E **90**, 052803 (2014).
[46] H. Liu, M. Zheng, D. Wu, Z. Wang, J. Liu, and Z. Liu, Phys. Rev. E **94**, 062318 (2016).
[47] C.-R. Cai, Z.-X. Wu, M. Z. Q. Chen, P. Holme, and J.-Y. Guan, Phys. Rev. Lett. **116**, 258301 (2016).
[48] Y. Zhou, J. Zhou, G. Chen, and H. E. Stanley, New J. Phys. **21**, 035002 (2019).
[49] J. P. Gleeson, Phys. Rev. Lett. **107**, 068701 (2011).
[50] J. P. Gleeson, Phys. Rev. X **3**, 021004 (2013).
[51] G. J. Ackland and I. D. Gallagher, Phys. Rev. Lett. **93**, 158701 (2004).
[52] R. Pastor-Satorras and A. Vespignani, Phys. Rev. Lett. **86**, 3200 (2001).
[53] G. A. Tsekouras and A. Provata, Phys. Rev. E **65**, 016204 (2001).
[54] R. Pastor-Satorras, C. Castellano, P. Van Mieghem, and A. Vespignani, Rev. Mod. Phys. **87**, 925 (2015).
[55] B. Bollobás, *Random Graphs*, 2nd ed. (Cambridge University Press, Cambridge, 2001).
[56] A. S. Mata, R. S. Ferreira, and S. C. Ferreira, New J. Phys. **16**, 053006 (2014).
[57] M. M. de Oliveira and R. Dickman, Phys. Rev. E **71**, 016129 (2005).
[58] S. C. Ferreira, C. Castellano, and R. Pastor-Satorras, Phys. Rev. E **86**, 041125 (2012).
[59] M. Boguñá, C. Castellano, and R. Pastor-Satorras, Phys. Rev. Lett. **111**, 068701 (2013).
[60] K. Wood, C. Van den Broeck, R. Kawai, and K. Lindenberg, Phys. Rev. Lett. **96**, 145701 (2006).
[61] K. Wood, C. Van den Broeck, R. Kawai, and K. Lindenberg, Phys. Rev. E **76**, 041132 (2007).
[62] T. Herpich and M. Esposito, Phys. Rev. E **99**, 022135 (2019).